ORGANOMETALLICS
Article
pubs.acs.org/Organometallics

Control of Chemoselectivity by Coordinated Water and Relative Size of Ligands to Metal Cations of Lewis Acid Catalysts for Cycloaddition of an Oxirane Derivative to an Aldehyde: Theoretical and Experimental Study

Ziqi Tian,[†] Yuanjing Xiao,[‡] Xiangai Yuan,[†] Zuliang Chen,[‡] Junliang Zhang,*[,‡] and Jing Ma*[,†]

[†]Key Laboratory of Mesoscopic Chemistry of MOE School of Chemistry & Chemical Engineering, Nanjing University 22 Hankou Road, Nanjing, 210093, People's Republic of China

[‡]Shanghai Key Laboratory of Green Chemistry and Chemical Processes Department of Chemistry, East China Normal University 3663 North Zhongshan Road, Shanghai 200062, People's Republic of China

Ⓢ *Supporting Information*

ABSTRACT: The role played by Lewis acid catalysts in the selective cleavages of C−O and C−C bonds of oxirane derivatives with aldehydes is investigated both theoretically and experimentally. According to the different chemoselectivities, various catalysts are divided into four series: C−O selectivity, both, C−C selectivity, and none, respectively. The involvement of coordinated water molecules is crucial to rationalize the experimental observation of C−C selectivity for the $Ni(ClO_4)_2·6H_2O$-catalyzed reaction, which is supported by experiment on changing originally unreactive $Ni(OTf)_2$ to be an effective catalyst by mixing with water. Furthermore, the steric hindrance from the anion in Lewis acid and the water molecule have significant influence on the efficiency of catalysts. A steric parameter, *α*, defined as the relative ratio of ligand size to radius of the center metal cation, gives a general picture to understand the selectivities of various Lewis acid catalysts. The ineffective $M(OTf)_2$ type catalysts have remarkable steric hindrance with $\alpha > 4.5$. Large cations ($R_M > 74$ pm) relative to their surrounding ligands with $\alpha < 4$ prefer the C−O bond cleavage path, while small cations ($R_M < 70$ pm) with $\alpha < 4.5$ lead to C−C bond breaking. An understanding of the relationship between selectivity and Lewis acid catalysts may guide the design of more selective and versatile Lewis acid catalysts for organic synthesis.

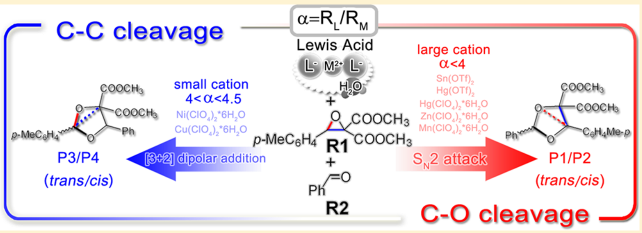

1. INTRODUCTION

Dipolar [3 + 2] cycloaddition reactions[1] are hot topics in organic chemistry due to their wide application in the synthesis of various compounds containing five-membered rings, the common skeletons in natural and pharmaceutical compounds.[2] In cycloaddition with 1,3-dipolar compounds, including oxirane derivatives containing three-membered rings,[3] many species with polarized double bonds are considered as dipolarophiles.[4] Oxiranes (for instance, aryloxiranyldicarboxylate, **R1**) have a propensity of strain-induced ring opening and two asymmetric centers; thus, they are very important reagents in numerous industrial processes and syntheses of natural products.[5] Nucleophilic ring opening by an S_N2 mechanism has been well recognized. However, without other reactants and catalysts, the calculated energy barrier (24.1 kcal/mol at the B3LYP/6-31+G(d) level) of C−C bond cleavage in **R1** is smaller than that (37.1 kcal/mol) of C−O cleavage, due to the evident polarity of the C−O bond relative to the C−C bond. As a result, selective C−O or C−C bond cleavage from the same substrates is an exciting challenge. In additions with aldehydes **R2**, C−O and C−C bonds of **R1** could be selectively cleaved by using different metal-centered Lewis acid catalysts,[6] as shown in Scheme 1.

Scheme 1. C−C vs. C−O Bond Cleavage

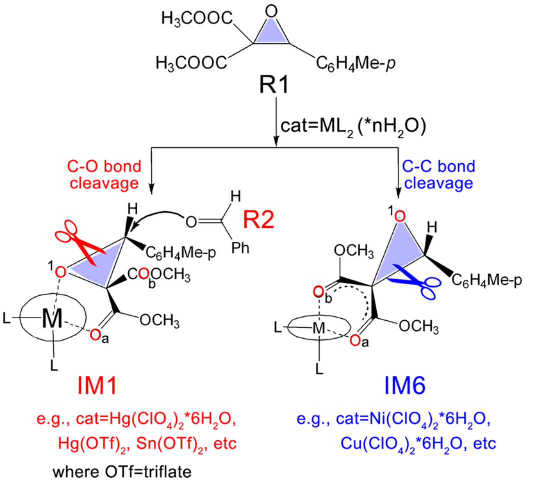

Received: January 22, 2014
Published: March 28, 2014

dx.doi.org/10.1021/om500068m | *Organometallics* 2014, 33, 1715−1725

According to the different chemoselectivities of catalyzed reactions for opening of oxirane by aldehyde,[6c] ML_2 ($\cdot nH_2O$) type catalysts (L= triflate or perchlorate, n = 1−6) could be classified into four series: (I) catalysts which lead to C−O bond cleavage only, called *C−O selectivity*, (II) catalysts with no selectivity for breaking C−O or C−C bonds, named as *both*, (III) catalysts which just favor C−C bond cleavage, i.e., *C−C selectivity*, and (IV) ineffective catalysts for both C−C and C−O bond breaking, labeled as *none*. The collection of the aforementioned experimental results, as shown in Figure 1, gives us an impetus to systematically study the role of Lewis acid catalysts in the control of selectivity.

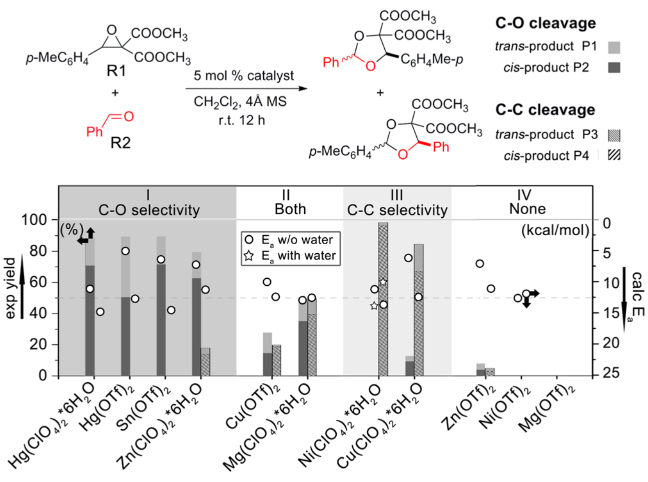

Figure 1. Classification of the ML_2 ($\cdot nH_2O$) type catalysts with respect to the selectivity. The experimental results in the plot are mainly taken from ref 6c.

Theoretical rationalizations of [3 + 2] dipolar cycloaddition reactions have been devoted to drawing possible reaction paths and explaining chemo- and stereoselectivities.[7] The qualitative description of addition processes by frontier molecular orbital (FMO) theory has been widely accepted. The dipolar [3 + 2] cycloaddition reactions have been further classified into three different types by Sustmann,[8] according to the character of the highest occupied molecular orbital (HOMO) and lowest unoccupied molecular orbital (LUMO) interactions in reactants. In this work, calculations will show that the studied catalytic reactions are mainly controlled by $LUMO_{dipole}$−$HOMO_{dipolarophile}$ interactions, which are different from those without catalysts, because the coordinated catalysts narrow the energy gaps between $LUMO_{dipole}$ and $HOMO_{dipolarophile}$. However, these calculations will show that the sole indicator of the HOMO−LUMO gap cannot account for the difference in chemoselectivities caused by different Lewis acid catalysts, especially for C−O selectivity. For those complicated reactions beyond the control of a simple FMO picture, density functional theory (DFT) was widely used to gain a more quantitative picture of reaction paths and corresponding activation energy barriers.[9] The catalytic effects of noble metals (for instance, the complexes of Rh, Pt, et al.)[10] and Lewis acids (such as the metallic salts and BF_3)[11] have been addressed theoretically. Despite these advances in the rationalization of chemo- and stereoselectivities, there are still some open questions for understanding all of the experiments. For example, whether the dipolar addition is stepwise or concerted is hotly debated.[12]

Recently, in cooperation with experiment of a series Lewis acid catalyzed reactions, we explored the possible reaction paths of $Sn(OTf)_2$-catalyzed reactions of **R1** with **R2**, as shown in Figure 2.[6c] It was supposed that C−O bond cleavage may proceed through an S_N2 pathway, in which nucleophilic aldehyde attacked oxirane from the back. As another possibility, the C−C bond may be weakened by the coordination of a Lewis acid.[13] This leads to thermal ring opening to generate a carbonyl ylide intermediate, which is an emblematic 1,3-dipole to react with dipolarophile. C−O and C−C bond cleavage pathways are always concomitant and competitive.

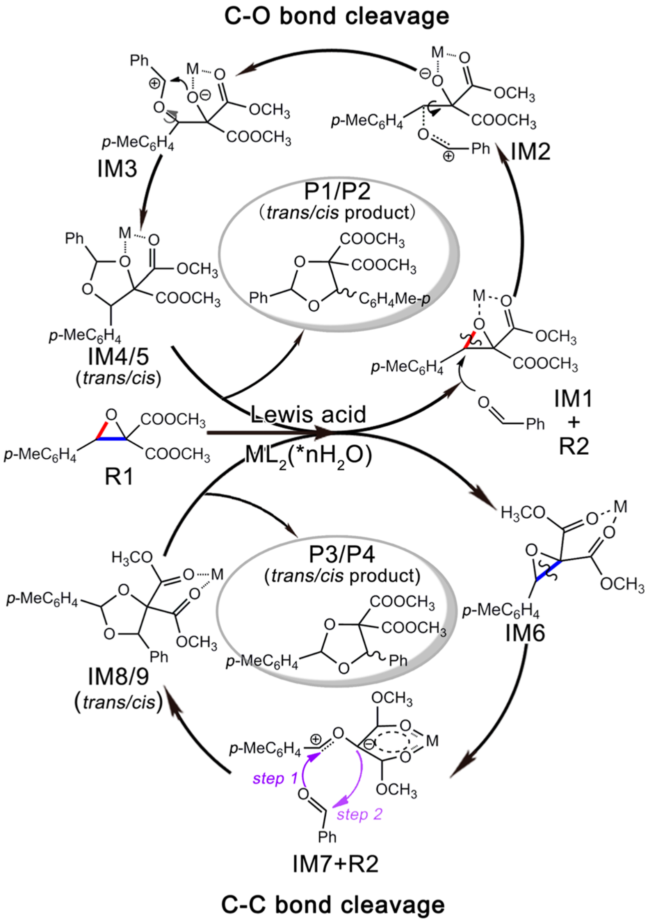

Figure 2. Possible C−O and C−C cleavage pathways. Ligands coordinated to metal ions are omitted for clarity.

Our recent calculations on $Sn(OTf)_2$-catalyzed reactions show that the activation energy barrier, E_a, for C−O cleavage is lower than that for C−C bond breaking, which is in good agreement with the experiment that $Sn(OTf)_2$-catalyzed reaction mainly produced the C−O bond cleaved products with about 90% yield.[6c] However, the nearly identical energy barriers of C−O vs C−C bond cleavage catalyzed by using ideal water-free $Ni(ClO_4)_2$ model catalysts, as depicted by the dots in Figure 1, cannot explain the evident selectivity in C−C bond breaking for the $Ni(ClO_4)_2\cdot 6H_2O$-catalyzed experiment. In the present work, we will show the important role of trace water in controlling the chemoselectivity brought by $Ni(ClO_4)_2\cdot nH_2O$. In fact, water molecules could participate in many organic processes as a reagent to accelerate reactions, such as the water-catalyzed [1,2]-hydrogen shift.[14] We will demonstrate that the E_a value of C−O bond cleavage increases when the coordinated water is involved in a $Ni(ClO_4)_2\cdot nH_2O$-catalyzed reaction, which is denoted by the star symbols in Figure 1. However, the energy barrier of C−C cleavage decreases, enhancing the preference for C−C bond cleavage. To give more evidence for our hypothesis of water-improved selectivity, some supplementary experiments have then been carried out by mixing additional trace water into the originally ineffective catalyst $Ni(OTf)_2$, from which C−C bond cleaved products are mainly obtained. Furthermore, a simple geometry indicator, defined as the relative size of the anion (including coordinated water molecules) with respect to that of the cation for the metal-centered Lewis acid catalysts, correlates well with the chemoselectivity for a broad range of Lewis acids, covering all four series of catalysts shown in Figure 1. Using the radii of cations and this indicator, we predict that the $Mn(ClO_4)_2$-catalyzed reaction may favor the C−O cleavage path, which is further supported by experiment.

2. THEORETICAL MODELS AND COMPUTATIONAL AND EXPERIMENTAL DETAILS

To understand the chemoselectivity of Lewis acid catalyzed cycloaddition reactions of **R1** with **R2**, possible reaction pathways (Figure 2) for the C−C and C−O cleavages were theoretically studied by using DFT, respectively. Some related experiments were also performed to test the theoretical predictions on selectivities of other catalysts.

2.1. Computational Details. All DFT calculations were carried out with the Gaussian09 program package.[15] The B3LYP functional[16] was employed for optimizations, with the standard 6-31+G(d) basis sets for nonmetal elements. The 6-311+G(d) full-electron basis set was used for Mg. For the other heavier metals, LANL2DZ effective core potentials were used.[17] An alternative functional, M06-2X,[18] was used to study the $Sn(OTf)_2$-catalyzed path to test the influence of different functionals (Figure S1, Supporting Information). The M06-2X functional result could give the same conclusion, that the C−O bond cleavage is favorable, as the B3LYP result and experiment. C−O bond cleavage was correctly predicted as the time-limiting step in the C−O path. While M06-2X requires more computational cost than B3LYP and gives some unreasonable structures (such as **IM2-Sn**, shown in Figure S1), the B3LYP functional is used in all the following computations. The stabilities of wave functions were also tested. The restricted methods were applicable for most species, except for those in manganic and nickelous salt catalyzed pathways. Taking $Ni(ClO_4)_2$ as an example, the geometries of its singlet and triplet were optimized by UB3LYP. High-spin $Ni(ClO_4)_2$ takes a tetrahedral geometry, while the low-spin complex tends to be a square-planar structure. The Gibbs free energy of the triplet is 7.5 kcal/mol energetically lower than that of the singlet. These intermediates containing Ni^{2+} were found to have strong interference in the NMR experiments, supporting that these nickel species preferred the high spin ground states. It can also be found from Figure S2 (Supporting Information) that the spin densities of the high-spin Lewis acid catalysts and reactive species are mainly localized on the metallic center. Frequency calculations were performed to test obtained stationary points, intermediates (**IM**), or transition states (**TS**) and to get their zero-point energies and other thermochemical corrections at 298 K. Only vibrational contributions to the thermal corrections were considered, because rotation and transition movements were highly suppressed in solution under the experimental conditions.[19] Single-point energies were computed at the B3LYP/6-311++G(d,p) level (SDD for metals[20]) with the SMD solvation model (dichloromethane solvent, ε = 8.9) at optimized geometries.[21] In discussions, Gibbs free energies of reaction pathways in solution will be employed in the rationalization of chemoselectivity of the [3 + 2] cycloaddition. In addition, natural bond orbital (NBO) calculations[22] were performed to show the partial atomic charges and localized molecular orbitals.

2.2. Experimental Details. To test the influence of trace water, a typical procedure was run as follows: in an inert-atmosphere glovebox, a flame-dried vial was charged with 5 mol % of $Ni(OTf)_2$ catalyst, 100 mg of activated 4 Å molecular sieves (MS), and a magnetic stir bar. Outside of the glovebox, the vial was placed under an N_2 atmosphere and charged with 1 mL of DCM, followed by **R2** (56 μL, 0.55 mmol). Afterward, **R1** (125 mg, 0.5 mmol) and 4 mL of DCM containing some H_2O were added. The reaction mixture was stirred at room temperature for 24 h. The reaction mixture was then passed over a plug of silica with 30 mL of Et_2O. The solvent was removed under reduced pressure, and the ratio of stereoisomers was determined by ^1H NMR spectroscopy using dibromomethane as the internal reference. For more details, see the Supporting Information and ref 6c.

3. RESULTS AND DISCUSSION

Without Lewis acid catalyst, both C−O and C−C bond cleavages are impossible at room temperature.[23] It will be demonstrated in section 3.1 that employment of many Lewis acid reagents does promote C−O and C−C bond cleavages. Through the consideration of coordinated water in $Ni(ClO_4)_2 \cdot 6H_2O$ on selectivity, we will also show in section 3.2 that trace water molecules tend to coordinate to metal cations, subsequently altering the height of the energy barriers and affecting the activity and selectivity of the catalyst. From the perspective of steric hindrance and electrostatic effects, we attempt to propose a geometry indicator to generalize the selectivity by using different Lewis acid catalysts.

3.1. Overview of $Sn(OTf)_2$-Catalyzed Pathway: C−O Cleavage Selectivity. Although some preliminary calculated results of $Sn(OTf)_2$-catalyzed reactions have been reported,[6c] some details of the energy profiles as well as the geometries of some important stationary points are crucial to gain a comprehensive picture of these reactions. In **R1**, it is possible for three oxygen atoms, represented as O1 (from oxirane ring) and Oa and Ob (from carbonyls) in Scheme 1, respectively, to coordinate with metal cations of Lewis acid catalysts. In **IM1**, the cation binds to the sp^3 oxygen (O1) of oxirane and one of the sp^2 oxygens of carbonyl groups (Oa or Ob), activating the C−O bond of oxirane. Alternatively, if the cation coordinates to two carbonyl groups to form **IM6**, C−C cleavage would occur.

As shown in Scheme 2, C−O bond cleavage follows an S_N2-like mechanism. **R2** attacks the benzyl carbon atom of **IM1-Sn**, leading to C−O bond cleavage and formation of a new C−O bond. There are two directions of attack for **R2**, the front and back of the cleaving C−O bond, as shown in Figure 3. As expected, an S_N2 reaction with the nucleophile group attacking the reaction center from the back of the leaving group is more favorable, with an energy barrier of about 6.5 kcal/mol. The dihedral angle O1−C2−C3−O4 of **TS1-Sn** is −167.5°, implying that it is going to form the gauche conformation intermediate **IM2-Sn**. It is very difficult to locate the rotation transition state before ring closure, due to the flat rotation potential energy surface. A scan of potential energy curves for rotation angle was performed to find the transition structure **TS2-Sn** with an eclipsed conformation (dihedral angles O1−C2−C3−O4 are nearly ±120° and energy barriers are estimated to be 8.5 and 9.4 kcal/mol, respectively). Taking into account the structure relaxation, the rotation energy barrier in the real reaction may be even lower than calculated barriers. In comparison with facile processes such as single-bond rotation and new bond formation between atoms with opposite charges, C−O bond cleavage from back attack is considered to be the rate-limiting step.

In **IM3-Sn**, C5 possesses a positive charge (0.47 au) and O1 (−0.98 au) has a negative charge; thus, the formation of a new bond between these two atoms is energetically favored with relatively low energy barriers of 3.7 and 2.4 kcal/mol for trans and cis paths, respectively. The cyclization would occur via transition states **TS3-Sn** (for trans) or **TS4-Sn** (for cis) with eclipsed conformations (dihedral angles O1−C2−C3−O4 are

Scheme 2. B3LYP Free Energy Profile for [3 + 2] Cycloaddition Reaction Paths Catalyzed by $Sn(OTf)_2$[a]

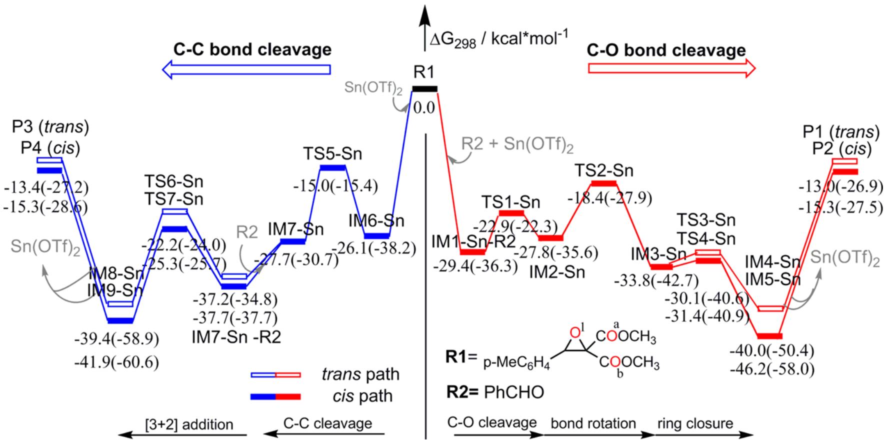

[a] The results calculated at the M06-2X/6-311++G(d,p)/SDD //M06-2x/6-31+G(d)/LAN2DZ level are also given in brackets.

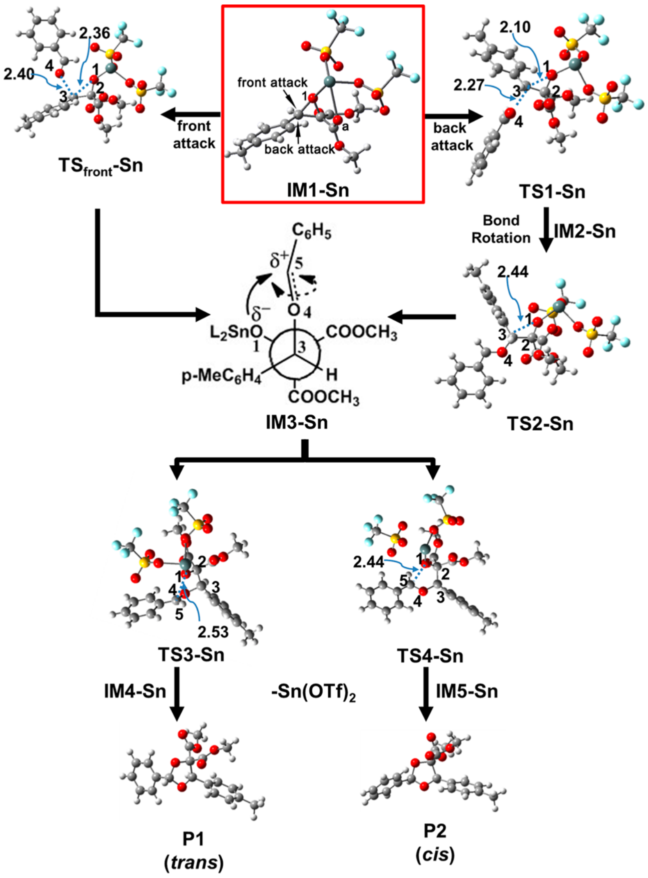

Figure 3. Optimized stationary point structures on the C−O bond cleavage path catalyzed by $Sn(OTf)_2$.

49.2 and 11.0°, respectively), shown in Figure 3. Going through **IM4-Sn** (**IM5-Sn**), trans (cis) product is obtained. The population ratio of cis and trans products is estimated to be 3.3 from Boltzmann statistic calculations. The possibility of reverse reactions is indicated by relatively low gaps of 9.9 and 14.8 kcal/mol for **TS3-Sn** → **IM4-Sn** and **TS4-Sn** → **IM5-Sn**, respectively. While these gaps are larger than the activation energy barrier of the time-limiting step of the forward reactions (no more than 10 kcal/mol), the reverse reactions from **IM4-Sn** and **IM5-Sn** to **IM3-Sn** are thus possible but are much slower than the forward reaction. Our models and calculations agree well with the experimental fact that the trans product **P1** could transform into the cis product **P2** when $Sn(OTf)_2$ is present.

C−C bond cleavage resembles a [3 + 2] addition mechanism. The C3−C2 bond of oxirane can be activated by catalyst coordination with two carbonyl groups, forming **IM6-Sn**. The energy barrier of C−C bond cleavage is 11.1 kcal/mol, higher than that (6.5 kcal/mol) for C−O cleavage. The broken-bond intermediate state **IM7-Sn** would be stabilized by charge transfer from $O1^{\delta-}$ to C2 and C3 atoms (**IM1-Sn** → **IM7-Sn**: −0.49 au → −0.02 au). In **IM7-Sn**, the plane determined by C3, O1, C2 and the plane determined by C2 and the two carbonyl groups are not strictly coplanar, with a dihedral angle of about 63.5°, implying a weak conjugation effect. After C−C bond cleavage, the activated site at C3 (with a charge of 0.03 au) of **IM7-Sn** is then attacked by the nucleophilic oxygen atom O4 (−0.54 au) of **R2**. Transition states **TS6-Sn** and **TS7-Sn** are going to generate trans and cis products, respectively, through formation of **IM8-Sn** and **IM9-Sn** intermediates (Figure 4). The activation energy barrier is 15.0 kcal/mol for trans addition and 12.4 kcal/mol for cis addition, greater than the barrier of C−C bond breaking pf 11.1 kcal/mol; hence, the addition step is also predicted to determine the reaction rate.

3.2. $Ni(ClO_4)_2 \cdot nH_2O$-Catalyzed Pathway: C−C Cleavage Selectivity.

3.2.1. Catalysis without Involvement of Coordination Water. The energy profile is shown in Figure 5a, and optimized structures of intermediates and transition states on reaction paths are displayed in Figure 6. In all of these nickelous species, Ni cations are at the coordinated octahedral centers of the complex. For the C−O bond cleavage step, the energy barrier is 11.2 kcal/mol, obviously higher than the C−O cleavage barrier catalyzed by $Sn(OTf)_2$ (6.5 kcal/mol). Thus, under similar experimental conditions, $Ni(ClO_4)_2$-catalyzed C−O cleavage is difficult to carry out. The rotation energy barrier from **TS2-Ni** to **IM3-Ni** is 6.8 kcal/mol. The potential energy surface near **IM3-Ni** is extremely flat. Although the structures of **IM3-Ni**, **TS3-Ni**, and **TS4-Ni** have very significant differences in the bond lengths of C3−C5 and dihedral angles, φ(C5−O4−C3−O1), their internal energies are almost the same. For the C−C bond cleavage path, C−C bond is cleaved from **IM6-Ni** to **TS5-Ni** with an energy barrier of 13.7 kcal/mol. In **IM7-Ni**, C3 and C2 both bear sp^2 hybrid orbitals. The two orbital planes of C3 and C2 are almost coplanar with an almost

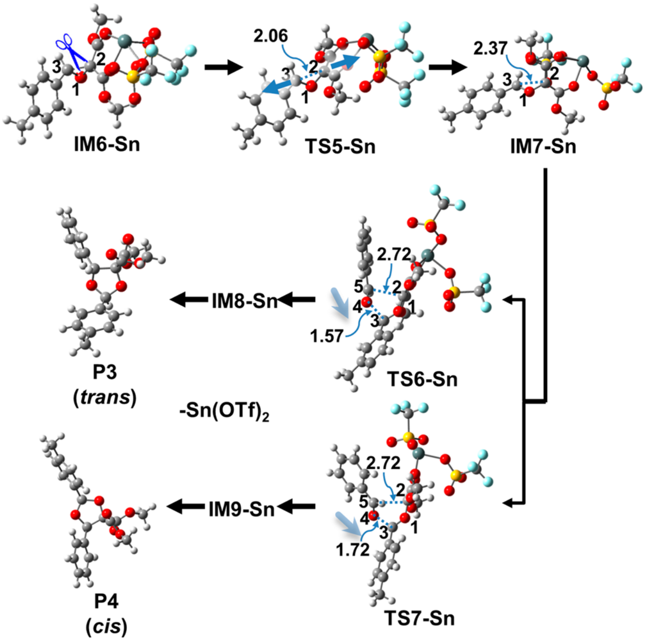

Figure 4. Species of C−C bond-cleavage reactions catalyzed by Sn(OTf)$_2$.

0° dihedral angle (0.90°) of two esters, which is much smaller than that (63.5°) in the Sn(OTf)$_2$-catalyzed path. Energy barriers of trans (from **IM7-Ni** to **TS6-Ni**) and cis (from **IM7-Ni** to **TS7-Ni**) addition steps are 15.8 and 8.8 kcal/mol, respectively. The energy difference between **TS6-Ni** (for trans) and **TS7-Ni** (for cis) is 7.0 kcal/mol, while for Sn(OTf)$_2$-catalyzed reaction, the energy difference between **TS3-Sn** (for trans) and **TS4-Sn** (for cis) is just 1.3 kcal/mol. This shows that Ni(ClO$_4$)$_2$ processes have stereoselectivity higher than those of Sn(OTf)$_2$. For Ni(ClO$_4$)$_2$-catalyzed paths, the barrier of the rate-limiting step for the C−O cleavage path is 11.2 kcal/mol, which is very close to that (13.7 kcal/mol) of the C−C path. Unfortunately, this does not agree with the experiment that only C−C bond cleavage products were obtained.

We may recall that in experiments nickel(II) perchlorate hexahydrate is used as a catalyst instead of anhydrous nickel(II) perchlorate, since the anhydrous salt is always dangerous in organic reactions. Although 4 Å molecular sieves are mixed in reaction systems for removing water, there may be still trace water in the system. The following calculations will reveal that trace water may coordinate to Ni^{2+} and change reaction energy barriers sensitively.

3.2.2. Effect of Trace Water. Ni^{2+} is at the center of an octahedron. **R1** occupies two coordination sites, and the remaining four sites can be occupied by other ligands: for instance, ClO_4^- and H_2O. ClO_4^- could be a chelating ligand by using two oxygen atoms (represented as η^2-ClO_4^-) or just a monodentate ligand (represented as ClO_4^-) if a water molecule occupies a coordination site. In other words, water of crystallization can replace one of the chelating oxygen atoms of the ClO_4^- group. As shown in Figure 5b, the other four **R1**-unoccupied coordination sites are marked a−d, respectively. For a water-free catalyst, two η^2-ClO_4^- ligands occupy the a−b and c−d sites, respectively. Ni(η^2-ClO$_4$)$_2$-**R1**, which has been calculated as **IM1** or **IM6**, has no geometric isomer but its own. However, for the single-water-coordinated complex (represent as $n = 1$ in the following), Ni(η^2-ClO$_4$)(ClO$_4$)OH$_2$-**R1**, there are four isomers denoted 1H$_2$Oa, 1H$_2$Ob, 1H$_2$Oc, and 1H$_2$Od, respectively. Similarly, Ni(ClO$_4$)$_2$(OH$_2$)$_2$-**R1** with two coordination water molecules ($n = 2$) should have six isomers, denoted 2H$_2$Oab, 2H$_2$Oac, 2H$_2$Oad, 2H$_2$Obc, 2H$_2$Obd, and 2H$_2$Ocd (Table S1, Supporting Information). The case with more substituted water molecules may be rare because of the following issues. First, if the third water molecule coordinates with Ni^{2+} and replaces one ClO_4^- group, the reactant complex cannot keep a nonzero total charge. Obviously the charge-separated system is difficult to form in a weak polar solvent, such as CH_2Cl_2 or toluene in our experiments. Second, the redundant water is actually more favorable to replace one coordination site of **R1** instead of ClO_4^-; thus, Ni(ClO$_4$)$_2$(OH$_2$)$_3$-(η^1-**R1**), an unreactive species, would appear instead of Ni(ClO$_4$)(OH$_2$)$_3$-**R1**. The third and perhaps the most important reason is that water is a typical dipolarophile; thus, the excess water may tend to attack the reactive site, leading to side reactions. (In experiments, 4 Å molecular sieves are used to remove excess water. Even a little more water may cause vicinal diol generation.)

Water in the reaction system tends to coordinate with Ni^{2+}. To compare the binding ability of water with Ni^{2+}, we define $\Delta E_{H_2O}^{IM1}$ ($\Delta E_{H_2O}^{IM6}$) as the energy differences generated by water coordination: i.e., $\Delta E_{H_2O}^{IM1} = E^{IM1}(\text{with } nH_2O) - E^{IM1}(\text{without } H_2O) - n[E(H_2O)]$. From the values of $\Delta E_{H_2O}^{IM1}$ and $\Delta\Delta E_{H_2O}^{IM6}$, we found that water replacing is extremely energetically favored, since a larger six-membered-ring structure having hydrogen bonds between the inserted water and ClO_4^- is formed (shown in the inset of Figure 5b and in Figure 6) instead of the chelating four-membered ring. The ideal coordination octahedron has three 4-fold symmetry axes. The average value, θ_{av}, of the three axial angles(such as ∠a−Ni−b in Figure 5b) can reflect distortion of the geometry from an ideal octahedron. Obviously, for an ideal octahedron, θ_{av} is 180°. The values of θ_{av} for **IM1** and **IM6** without coordinated water are 165.1 and 165.4°, respectively. Water coordination keeps the octahedral configuration. When $n = 1$, the θ_{av} values for **IM1** and **IM6** increase to 167.1 and 168.8° and further to 172.2 and 175.5° if $n = 2$, implying reinforced orbital overlap between nickel and ligand orbitals and a weakened stretch.

For C−O cleavage, if $n = 1$, 1H$_2$Oc leads to the largest value of $\Delta E_{H_2O}^{IM1}$ (14.8 kcal/mol), indicating the largest population in the single-water-coordinated complexes. For the 1H$_2$Oc-catalyzed pathway, the activation energy barrier for C−O bond cleavage (13.7 kcal/mol) is higher than that without water (11.2 kcal/mol) and any other single-water-coordinated paths. Similarly, for $n = 2$, complexes 2H$_2$Oab and 2H$_2$Ocd have relatively large value of $\Delta E_{H_2O}^{IM1}$ (26.8 and 26.7 kcal/mol, respectively), and C−O cleavage energy barriers are 13.9 and 13.3 kcal/mol, also higher than the non-water-coordinated energy barrier (11.2 kcal/mol). Thus, water coordination may weaken the tendency for C−O bond cleavage. On the other hand, for the C−C bond cleavage path, we considered the water-coordinated influence on both the C−C bond cleavage and [3 + 2] addition steps. Complexes 1H$_2$Ob and 2H$_2$Oab on the C−C cleavage path are the dominant species with $\Delta E_{H_2O}^{IM6}$ values of 13.2 and 28.6 kcal/mol, respectively. When $n = 1$, for 1H$_2$Ob, the energy barrier of C−C bond cleavage decreases from 13.7 to 10.0 kcal/mol. In addition, when $n = 2$ as 2H$_2$Oab, this energy barrier is 11.6 kcal/mol. Simultaneously, energy barriers of cycloaddition leading to cis product change slightly, from 8.8 to 8.9 kcal/mol for 1H$_2$Ob or 9.3 kcal/mol for 2H$_2$Oab. In contrast, energy barriers leading to trans product rise relatively obviously by about 4 kcal/mol (19.1 kcal/mol for $n = 1$, and 16.8 kcal/mol for $n = 2$), enhancing stereoselectivity.

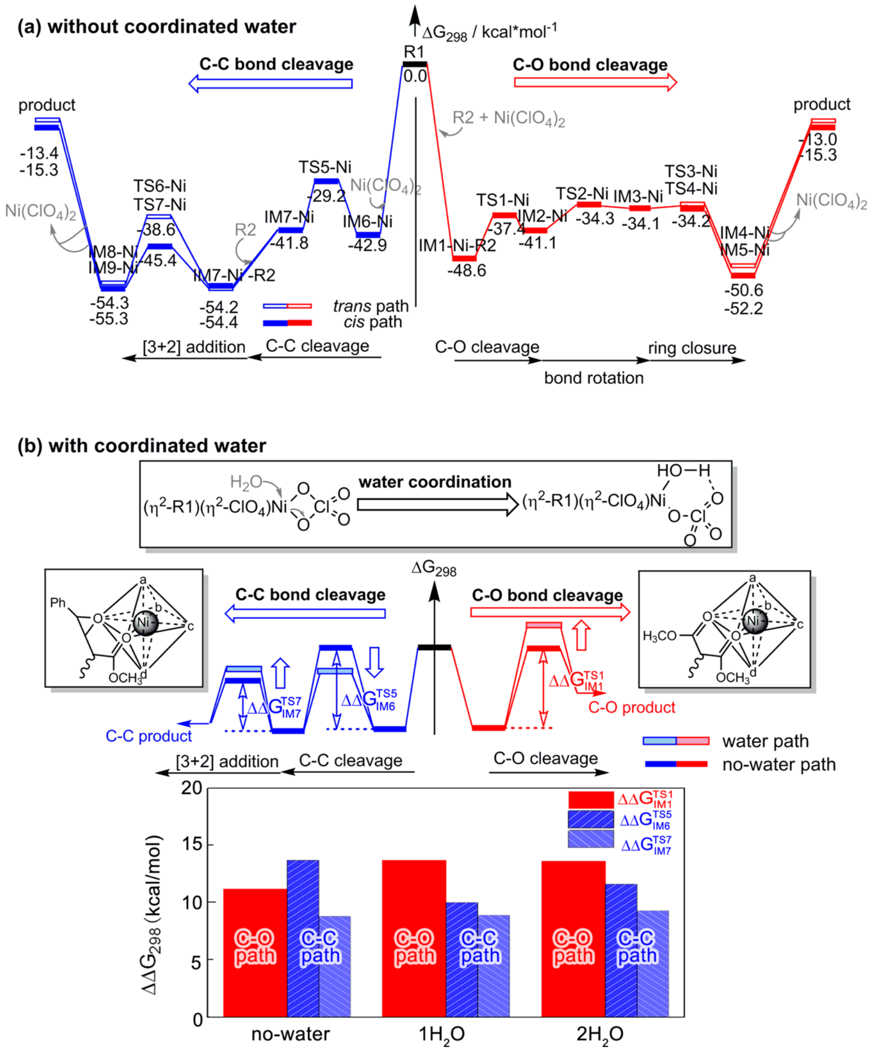

Figure 5. Free energy profile for [3 + 2] cycloaddition reaction paths catalyzed by $Ni(ClO_4)_2 \cdot nH_2O$ (a) without and (b) with the consideration of water coordination. All energies (in kcal/mol) are computed at the UB3LYP/6-311++G(d,p)/SDD//UB3LYP/6-31+G(d)/LANL2DZ level with SMD model for CH_2Cl_2 solvent. $\Delta\Delta G^{TSi}_{IMi}$ is the change in energy barrier from **IM*i*** to **TS*i***.

With consideration of water, energy barriers heights of C−C bond cleavage (10.0 kcal/mol) and [3 + 2] cis addition (8.9 kcal/mol) are comparable to each other. It can be conceived that lowering of the activation barrier in either the C−C cleavage or [3 + 2] addition step may promote reaction activity. In experiments, it was also found that electron-withdrawing substituents on oxiranes, e.g., two carboxyl groups in **R1**, are necessary for the reactant to facilitate C−C bond breaking and, alternatively, electron-donating groups on benzaldehyde, which increase the nucleophilicity of R2 and decrease the energy barrier of addition, can also accelerate the reaction.[6c] In summary, for water-coordinated nickel(II) complexes, energy barriers of C−O bond cleavage rise, while barriers of C−C cleavage and [3 + 2] *cis* addition decrease or change slightly, which indicates that water coordination may change the chemoselectivity and stereoselectivity of the Lewis acid catalyst.

Furthermore, we calculated the activation energy barriers of the rate-limiting step for $Ni(OTf)_2$-catalyzed pathways to investigate the role of trace water further. $Ni(OTf)_2$ is an ineffective catalyst for both C−O and C−C cleavage in experiments (Figure 1). Without the consideration of water, Ni^{2+}-catalyzed reactions have similar energy barriers whether the ligand is OTf^- or ClO_4^-. When an appropriate amount of water was added (Table 1), $Ni(OTf)_2$ showed a moderate catalytic effect in DCM in the presence of molecular sieves. The control experiments further support our hypothesis that trace water can enhance the catalytic activity and lower the activation energy of C−C bond cleavage.

It is also possible that water may be the source of protons that promote the reaction. The control experiments with 5 mol % TfOH also rule out the possibility that the proton (which may come from water) can catalyze the [3 + 2] cycloaddition reaction involving both C−O and C−C bond cleavage (eq 1 in Scheme 3). Interestingly, when 2,6-di-*tert*-butylpyridine was added to the standard reaction conditions, neither C−O nor C−C cleavage cycloaddition products could be obtained. This indicated that 2,6-di-*tert*-butylpyridine may coordinate to the nickel cation, resulting in ineffective catalysis (eq 2 in Scheme 3).

3.3. General Trends in Chemoselectivity of Lewis Acid Catalyzed Reactions.

Versatile Lewis acid catalyzed reactions have been applied to many important processes in organic synthesis.[24] In most cases, various types of Lewis acid catalysts have been screened after trial and error, due to limited knowledge of the electronic character of the Lewis acid. Thus, an in-depth understanding about the role of Lewis acid catalysts is necessary for designing various chemoselective reactions. There are some general classifications of Lewis acids according

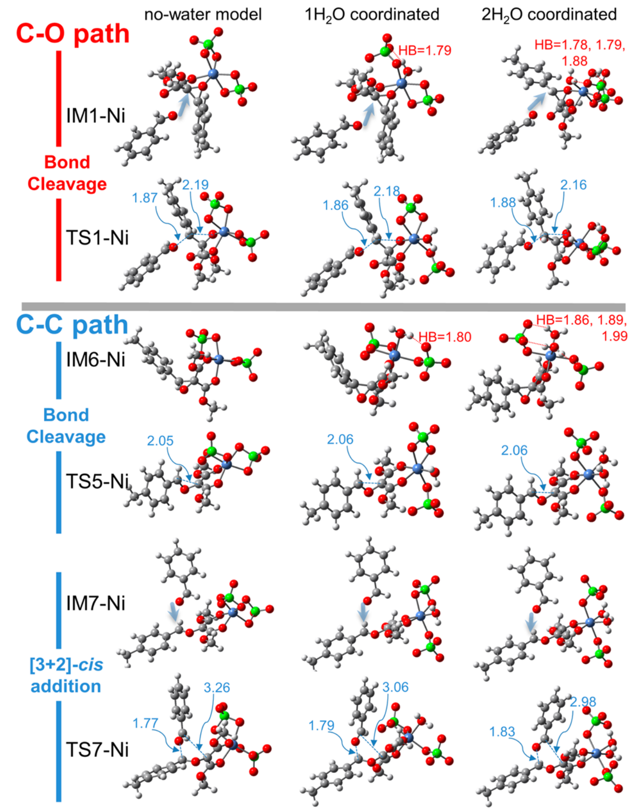

Figure 6. Optimized structures on the Ni(ClO$_4$)$_2$·xH$_2$O (x = 0−2) pathways. Selected bond lengths are given in angstroms, and the lengths of hydrogen bonds (HB) are also shown.

Table 1. Effect of Trace Water on Ni(OTf)$_2$-Catalyzed Reaction[a]

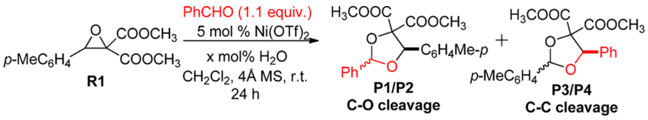

entry	x (mol % H$_2$O)	yield (%)[b]	
		P1 and P2	P3 and P4
1	0	0	0
2	10	0	trace
3	20	trace	28
4	30	trace	80

[a] [**R1**] = 0.1 M. [b] Estimated by ^{1}H NMR spectroscopy using dibromomethane as the internal reference.

Scheme 3. Control Experiment To Validate Water Effect

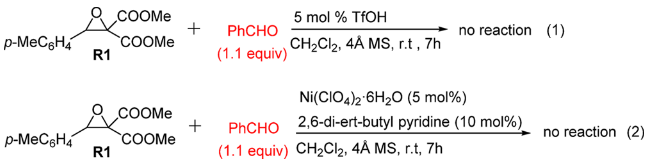

to the classical HSAB (hard and soft acids and bases) theory,[25] the catalytic effect on Friedel−Crafts or other reactions,[26] σ and π electrophilic properties,[27] etc. Here, we will address general trends in Lewis acid catalyzed cycloaddition reactions from both geometry considerations and FMO.

3.3.1. Geometry Indicators of Catalysts: Relative Size of Ligands vs Metal Cation. ML$_2$ type catalysts with bivalent cations (Ni^{2+}, Mg^{2+}, Cu^{2+}, Zn^{2+}, Hg^{2+}, Sn^{2+}) can be classified into four types according to chemoselectivity. A relationship between the effective cationic radius, R_M,[28] and chemoselectivity is presented in Table 2. The cations are hexacoordinated and are at the centers of octahedra with ∠O−M--O angles of about 90°. For the C−O bond cleavage path, the metal cation coordinates to **R1** to form a distorted five-membered ring with relatively longer M−O bonds. For example, in **IM1-Sn**, the lengths of two Sn−O bonds are 2.43 and 2.62 Å, respectively. However, for C−C bond cleavage, the cation is a part of a planar six-membered ring to make the redundant charge delocalized on the carbon atom of oxirane. Thus, a cation with small radius (R_M < 70 pm, such as Ni^{2+}) may prefer C−C bond cleavage; in contrast, a large cation (R_M > 74 pm, such as Sn^{2+} and Hg^{2+}) prefers C−O bond cleavage.

Table 2. Relationship between Chemoselectivity and Average Spatial Hindrance from the Ligands, Including Acid Anion (α_{ligand}) and Water Molecule (α_{water}), Relative to the Size of the Active Metal Center (R$_M$) in Lewis Acid Catalysts

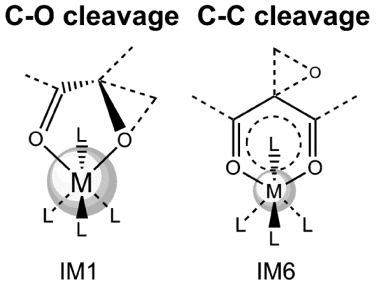

catalyst	R_M (pm)	α_{ligand}	α_{water}	$\bar{\alpha}$	selectivity	C−O:C−C yield (%)[a]
Sn(OTf)$_2$	112	3.5		3.5	C−O	90:0
Hg(ClO$_4$)$_2$·6H$_2$O	102	3.3	2.6	3.0	C−O	89:0
Hg(OTf)$_2$	102	3.8		3.8	C−O	90:0
Mn(ClO$_4$)$_2$·6H$_2$O	84	4.0	3.2	3.6	C−O	78:21
Zn(ClO$_4$)$_2$·6H$_2$O	74	4.5	3.6	4.0	C−O	80:18
Mg(ClO$_4$)$_2$·6H$_2$O	72	4.7	3.7	4.2	both	48:50
Ni(ClO$_4$)$_2$·6H$_2$O	69	4.9	3.9	4.4	C−C	0:99
Mn(OTf)$_2$	84	4.7		4.7	none	
Zn(OTf)$_2$	74	5.3		5.3	none	
Mg(OTf)$_2$	72	5.4		5.4	none	
Ni(OTf)$_2$	69	5.7		5.7	none	

[a] Most of experimental yields have been reported in ref 6c except that using Mn(ClO$_4$)$_2$*6H$_2$O and Mn(OTf)$_2$, which are added in this work.

From Table 2, it can be seen that the selectivity not only relates to R_M but also to the size of surrounding ligands relative to the cation. Intuitively, the spatial hindrance from ligands, including acid anion and water molecule, is also responsible for the catalytic reactivity. The large ligand may bury the cation and inhibit the coordination between cation and **R1**, leading to weak reactivity. Trace water in the reaction system may also coordinate to the cation to disturb the surroundings of the anion ligand. The sizes of water and other anion ligands can be estimated with *volume* keyword by using Gaussian 09 software. The radius, R, of water (R_{water} = 266 pm) is smaller than those (R_{OTf^-} = 391 pm, $R_{ClO_4^-}$ = 335 pm) of employed anions in this work. As a result, water replacement of the anions may weaken hindrance from the anion ligand. We set $\alpha_{ligand} = R_{ligand}/R_M$ as a parameter to measure the steric hindrance from the anion

Scheme 4. Experimental Result of $Mn(ClO_4)_2{\cdot}6H_2O$- and $Mn(OTf)_2$-Catalyzed Reactions

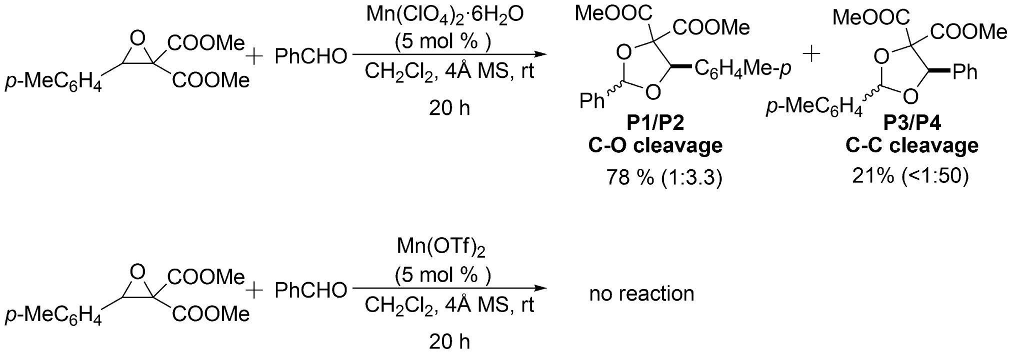

ligand. For Hg^{2+}, Zn^{2+}, and Mg^{2+} cations, the inner atom orbitals are fully filled with electrons; thus, they are all tetracoordinated with two anions in the centers of tetrahedra without coordination water or hexacoordinated with anions and coordination water molecules in the centers of octahedrons. In spite of the fact that Ni^{2+} has a d^8 configuration, the high-spin nickel complexes also have the structures similar to those mentioned above. Since ClO_4^- and OTf^- are both weak-field ligands, coordinate bonds are mainly formed by the outer orbitals of Ni^{2+} and orbitals from the ligands. In order to further consider the effect of water coordination, α_{water} (R_{water}/R_M) was also set. The average ligand hindrance, $\bar{\alpha}$, from anion and water coordination is evaluated as $0.5(\alpha_{ligand} + \alpha_{water})$, because in the tetrahedral coordination, water molecules and anions occupy two coordinated sites, respectively. The catalyst with a small cation ($R_M < 70$ pm) and relatively small value of $\bar{\alpha}$ ($\bar{\alpha} < 4.5$) tend to favor C–C cleavage. However, a $\bar{\alpha}$ value that is too small always corresponds to large R_M (such as $Sn(OTf)_2$, $\alpha = 3.5$ and $R_M = 112$ pm), leading to C–O cleavage. The larger the $\bar{\alpha}$ value is, the weaker the catalyzed effect and chemoselectivity. If $\bar{\alpha} > 4.5$, the catalyst may be ineffective for cycloaddition. Thus, the catalysts with ClO_4^- anions often have reactivity higher than that with the more space-demanding OTf^- group.

Cu^{2+} is a special case due to its d^9 configuration. The tetracoordinated Cu^{2+} is always at the center of a square plane. For these planar complexes, such as $Cu(OTf)_2$, hindrance along the axis is weak. Thus, although Cu^{2+} has a size (73 pm) similar to that of Mg^{2+} (72 pm), the steric hindrance from ligands may be weaker than for the corresponding magnesium salt. $Cu(OTf)_2$ is a catalyst with no selectivity, the same as $Mg(ClO_4)_2{\cdot}6H_2O$ ($\bar{\alpha} = 4.2$) but different from the ineffective $Mg(OTf)_2$ ($\bar{\alpha} = 5.4$) catalyst. However, for $Cu(ClO_4)_2{\cdot}6H_2O$, crystalline water molecules may coordinate to Cu^{2+} from the axial direction, generating the hexa-oordinated Cu^{2+}. In consideration of various possible coordination modes ranging from $4ClO_4/2H_2O$ to $2ClO_4/4H_2O$, the average ligand hindrance indictor, $\bar{\alpha}$, is estimated to be 4.3–3.9. Actually, $Cu(ClO_4)_2{\cdot}6H_2O$ has a catalytic selectivity for C–C bond breaking similar to that of $Ni(ClO_4)_2{\cdot}6H_2O$ ($\bar{\alpha} = 4.4$).

It is also interesting to test whether the cations with non-zero-spin preference, such as Ni^{2+} and Cu^{2+}, complicate the reaction mechanism and hence challenge the application of such a simple geometry indicator, α_{ligand}. The spin density distributions of the bond-breaking transition state (**TS5-Ni**) and ylide intermediate (**IM7-Ni**) on the $Ni(ClO_4)_2$-catalyzed path (Figure S2, Supporting Information) have been analyzed, showing that spin densities are mainly located on metal centers without significant spin polarization and delocalization. To test our guess the geometry is dominant, rather than spin preference, in controlling chemoselectivity, we implemented an experiment on $Mn(ClO_4)_2{\cdot}6H_2O$- and $Mn(OTf)_2$-catalyzed reactions. Mn^{2+} is a typical high-spin cation with a ground-state spin multiplicity of 6 in triflate or perchlorate salts. R_{Mn} is 84 pm, larger than that of Zn^{2+}. According to the geometry indicator, $Mn(ClO_4)_2{\cdot}6H_2O$ is predicted to have C–O selectivity (Table 2), which is supported by experiment that the yield of C–O cleavage products is about 78% (Scheme 4). However, for $Mn(OTf)_2$, α is 4.7 and this salt is an ineffective catalyst in experiment.

*3.3.2. Shifts of Energy Levels of **R1** by Catalysts.* FMO theory has been widely used to describe the catalyst effects on reaction paths.[8] Catalyst effects are usually rationalized from the variations of FMO of **R1**, especially $LUMO_{\mathbf{R1}}$. The LUMOs that localized at C–C and C–O bonds are mainly assigned as antibonding σ^* type. For the C–O cleavage path, $HOMO_{\mathbf{R2}}$ interacts with $LUMO_{\mathbf{R1}}$ (or $LUMO_{\mathbf{IM1}}$). A narrower $HOMO_{\mathbf{R2}}$–$LUMO_{\mathbf{R1}}$ energy gap ($HOMO_{\mathbf{R2}}$–$LUMO_{\mathbf{IM1}}$ after catalyst coordination) predicts a lower activation energy for C–O cleavage. In comparison, the first step of the C–C cleavage path is bond breaking of **R1**. If the $HOMO_{\mathbf{R1}}$–$LUMO_{\mathbf{R1}}$ energy gap ($HOMO_{\mathbf{IM6}}$–$LUMO_{\mathbf{IM6}}$ after catalyst coordination) is lowered by the catalyst, the thermal C–C bond cleavage may proceed, and **IM6** turns out to be **IM7/8** via **TS6**. Subsequently, the addition of **IM7** with **R2** occurs, and the $HOMO_{\mathbf{R2}}$–$LUMO_{\mathbf{IM7}}$ energy gap determines the reactivity of cycloaddition. We labeled energy gaps corresponding to C–C and C–O bond-breaking and [3 + 2] addition steps in Table 3. Apparently, $Sn(OTf)_2$ decreases the $HOMO_{\mathbf{R2}}$–$LUMO_{\mathbf{IM1}}$ energy gap for C–O cleavage (from 6.16 eV without catalyst to 2.62 eV). However, $Ni(ClO_4)_2$, especially coordinated with one water molecule, improves C–C cleavage, which is in accord with experiment and theoretical calculations. For other Lewis acid catalysts, FMO results can also give qualitative predictions for selectivity. The reaction tendency for C–O bond cleavage may be underestimated from the $HOMO_{\mathbf{R2}}$–$LUMO_{\mathbf{R1}}$ energy gap, partially because the S_N2 mechanism is not solely dependent on the HOMO and LUMO.

3.3.3. Stepwise or Concerted? A great number of studies have focused on whether [3 + 2] addition is concerted or stepwise.[12] Mongin et al.[12a] investigated the cycloaddition of oxirane derivatives with aldehydes by experiment and calculation. They proposed that electrophilically activated oxiranes reacted with aldehydes concertedly because of the reverse charge transfer from oxiranes to aldehydes. In our work, there are also electrophilic substitutions (such as C=O) on oxiranes to activate the C–C bond. By thermal excitation, the

Table 3. Some Important Energy Gaps of Different Lewis Acid Catalysts for the C−O and C−C Cleavages

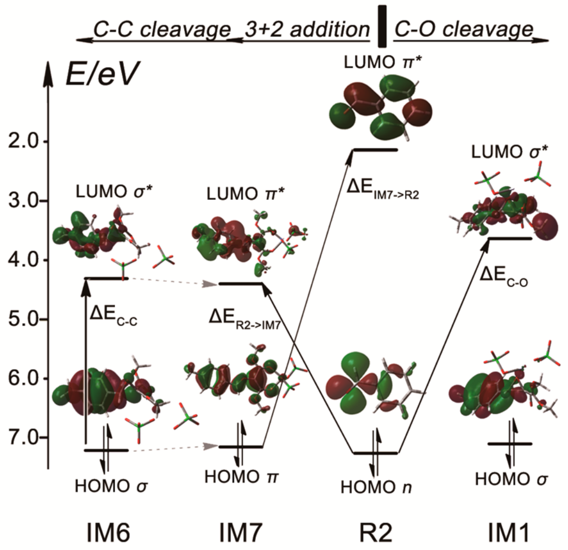

catalyst	C−O path $\Delta E_{\text{C−O}}$ (eV)[a]	C−C path $\Delta E_{\text{C−C}}$ (eV)[b]	$\Delta E_{\text{R−IM}}$ (eV)[c]	$\Delta E_{\text{IM−R}}$ (eV)[d]	selectivity
none	6.16	5.59	4.32	3.59	C−C
$Sn(OTf)_2$	2.62	2.82	2.65	4.68	C−O
$Hg(ClO_4)_2$	3.75	3.09	3.56	4.67	C−O
$Hg(OTf)_2$	4.20	3.10	3.71	4.31	C−O
$Zn(ClO_4)_2$	3.72	4.75	3.59	4.44	C−O
$Mg(ClO_4)_2$	4.73	2.92	2.90	5.04	both
$Cu(OTf)_2$	5.04	3.27	3.92	4.46	both
$Ni(ClO_4)_2$	3.66	2.93	2.90	5.06	C−C
$Cu(ClO_4)_2$	4.86	3.55	3.48	4.64	C−C
$Ni(OTf)_2$	3.69	4.74	2.97	4.97	none
$Zn(OTf)_2$	4.73	3.25	3.53	4.55	none
$Ni(ClO_4)_2 \cdot nH_2O$[e]					
$n = 1$	4.81	2.81	2.95	4.89	C−C
$n = 2$	4.73	2.85	3.96	4.44	C−C

[a] $\Delta E_{\text{C−O}} = E(\text{LUMO}_{\text{IM1}}) - E(\text{HOMO}_{\text{R2}})$. [b] $\Delta E_{\text{C−C}} = E(\text{LUMO}_{\text{IM6}}) - E(\text{HOMO}_{\text{IM6}})$. [c] $\Delta E_{\text{R−IM}} = E(\text{LUMO}_{\text{IM7}}) - E(\text{HOMO}_{\text{R2}})$. [d] $\Delta E_{\text{IM−R}} = E(\text{LUMO}_{\text{R2}}) - E(\text{HOMO}_{\text{IM7}})$. [e] Calculation with water coordination.

C−C bond of **R1** may cleave to form an ylide, represented as **R1**-ylide. This ylide is a typical 1,3-dipole to add to aldehydes. The $\text{HOMO}_{\text{R1-ylide}}$−$\text{LUMO}_{\text{R2}}$ energy gap (3.59 eV) is close to that (3.73 eV) of HOMO_{R2}−$\text{LUMO}_{\text{R1-ylide}}$, which indicates that charge transfer between the dipole and aldehyde is possibly bidirectional and cycloaddition may be concerted. A previous study showed that there exists reverse net charge transfer in a reaction similar to cycloaddition of thermally opened ylide with aldehyde.[12a] However, if **R1** coordinates with the catalyst (taking $Ni(ClO_4)_2$ as an example), the energies of the HOMO and LUMO of the complexes both decrease; thus the HOMO_{R2}−LUMO_{IM7} energy gap (2.89 eV) is smaller than that (5.06 eV) of HOMO_{IM7}−LUMO_{R2}, leading to unidirectional charge transfer from **R2** to **IM7**. On the other hand, the orbital phase of **R2** does not match that of **IM7**, weakening the tendency for concerted cycloaddition. During the calculation of the reaction step of addition, we found that it was hard to locate a local minimum without any imaginary frequency after C−O bond formation. Once the imaginary frequency with vibration mode of C−O formation was eliminated, the other vibration mode representing ring closure arose immediately. For these Lewis acid catalyzed reactions, [3 + 2] addition steps may still exhibit stepwise character, although ring-opening transition states have hardly been located.

4. CONCLUSION

Chemoselectivity of the Lewis acid catalyzed cycloadditions of aryloxiranedicarboxylates with aldehydes have been systematically investigated through theoretical calculations. C−O and C−C bonds of oxirane may be cleaved using different catalysts. We divided $ML_2 \cdot nH_2O$ type catalysts into four series based on chemoselectivity: *C−O selectivity*, *both*, *C−C selectivity*, and *none*.

C−O bond cleavage occurs via an anti attack as an S_N2 reaction, while the C−C bond is cleaved to form a polar ylide intermediate and then cycloaddition proceeds. For the C−C cleavage path, the energy difference between transition states leading to the cis and trans products are often larger than that in the C−O cleavage, indicating better steroselectivity. The coordinated water plays an important role in tuning the selectivity of the $Ni(ClO_4)_2$-catalyzed reaction. It was found that water coordination increases the energy barrier of C−O bond cleavage but decreases that of C−C bond cleavage. In our experiment, $Ni(OTf)_2$ can change from an inactive species to a C−C bond selective catalyst with the addition of some trace water, showing the unexpected effect of water.

The general trends of the Lewis acid catalyzed cycloaddition has been discussed from the perspective of both geometries of catalysts and FMO. It is suggested that a divalent cation with a large radius ($R_M > 74$ pm, such as Sn^{2+} and Hg^{2+}) in Lewis acids tend to catalyze C−O bond cleavage. If a cation (such as Ni^{2+}) is small, its surrounding anion in Lewis acid may prevent the coordination of the cation with the reactant, weakening the catalytic effect. The size of the coordinated anion will play a critical role in selectivity and efficiency. A geometry parameter, α, is defined to measure the steric hindrance from ligands. A large value of α indicates significant hindrance and vice versa. A catalyst with a small cation ($R_M < 70$ pm) and little steric hindrance ($\alpha < 4.5$) may be effective for C−C cleavage, while those catalysts with large values of α ($\alpha > 4.5$) are often inactive. A coordinated water molecule may lead to improved catalyst efficiency and chemoselectivity by reducing the ligand hindrance relative to the surrounding large anion ligand.

Using FMO theory, a qualitative picture can also be obtained to describe the selectivities of different catalysts. The energy gaps between LUMO_{IM6} and HOMO_{IM6} determine the energy barriers of C−C bond cleavage, while gaps between LUMO_{R2} and HOMO_{IM1} may partially correspond to the energy barriers of C−O bond cleavage. From the orbital phases of **IM7** and **R2**, it is suggested that cycloaddition is not concerted but stepwise. An understanding of the relationship between catalyst selectivity and cations, ligands, and coordinated water of Lewis acids may have interesting implications in the development of versatile Lewis acid catalyzed reactions.

■ ASSOCIATED CONTENT

Ⓢ Supporting Information

Figures S1−S5, giving optimized structures on $Sn(OTf)_2$-catalyzed paths at the M06-2X/6-31+G(d)/LANL2DZ level, spin density distributions of several nickelous complexes of high-spin states, energy profile of the front and back attacks for the $Sn(OTf)_2$-catalyzed C−O cleavage path, structures of various Lewis acid catalysts, and structures of species on the

$Ni(ClO_4)_2$-catalyzed path, Tables S1−S3, giving detailed information on the energy barriers of the water coordinated and various Lewis acid catalyzed paths, text giving experimental details for $Ni(OTf)_2$-catalyzed cycloaddition reactions and ^1H NMR spectra, and tables giving Cartesian coordinates for all the structures in this paper. This material is available free of charge via the Internet at http://pubs.acs.org.

■ AUTHOR INFORMATION

Corresponding Authors

*E-mail for J.Z.: jlzhang@chem.ecnu.edu.cn.
*E-mail for J.M.: majing@nju.edu.cn.

Notes

The authors declare no competing financial interest.

■ ACKNOWLEDGMENTS

This work was supported by the National Basic Research Program (Grant No. 2011CB808600) and the National Natural Science Foundation of China (Grant Nos. 21290192 and 21273102). We are grateful to the High Performance Computing Center of Nanjing University for doing the quantum chemical calculations in this paper on its IBM Blade cluster system.

■ REFERENCES

(1) For the earliest studies on the [3 + 2] dipolar cycloaddition, see: (a) Huisgen, R.; Bayer, H. O.; Schaefer, F. C.; Gotthardt, H. *Angew. Chem., Int. Ed.* **1964**, *3*, 136−137. (b) Huisgen, R.; Otto, P. *Tetrahedron Lett.* **1968**, 4491−4495. (c) Huisgen, R.; Brunn, E.; Gilardi, R.; Karle, I. *J. Am. Chem. Soc.* **1969**, *91*, 7766−7767.

(2) For recent leading reviews on the [3 + 2] dipolar cycloaddition: (a) Padwa, A.; Pearson, W. H. *Synthetic applications of 1,3-dipolar cycloaddition chemistry toward heterocycles and natural products*; Wiley: Hoboken, NJ, 2002. (b) Gothelf, K. V.; Jorgensen, K. A. *Chem. Rev.* **1998**, *98*, 863−909. (c) Fruhauf, H.-W. *Coord. Chem. Rev.* **2002**, *230*, 79−96. (d) Kanemasa, S. *Synlett* **2002**, 1371−1387. (e) Pandey, G.; Banerjee, P.; Gadre, S. R. *Chem. Rev.* **2006**, *106*, 4484−4517. (f) Nair, V.; Suja, T. D. *Tetrahedron* **2007**, *63*, 12247−12275. (g) Pellissier, H. *Tetrahedron* **2007**, *63*, 3235−3285. (h) Rubin, M.; Rubina, M.; Gevorgyan, V. *Chem. Rev.* **2007**, *107*, 3117−3179. (i) Patil, N. T.; Yamamoto, Y. *Chem. Rev.* **2008**, *108*, 3395−3442. (j) Carson, C. A.; Kerr, M. A. *Chem. Soc. Rev.* **2009**, *38*, 3051−3060. (k) Bartok, M. *Chem. Rev.* **2010**, *110*, 1663−1705. (l) Xing, Y.; Wang, N.-X. *Coord. Chem. Rev.* **2012**, *256*, 938−952.

(3) For examples of dipolar cycloadditions of aldehydes, see: (a) Christie, S. D. R.; Davoile, R. J.; Elsegood, M. R. J.; Fryatt, R.; Jones, R. C. F.; Pritchard, G. J. *Chem. Commun.* **2004**, 2474−2475. (b) Nair, V.; Mathai, S.; Viji, S.; Mathew, S. *Res. Chem. Intermediat.* **2006**, *32*, 1−7. (c) Pohlhaus, P. D.; Sanders, S. D.; Parsons, A. T.; Li, W.; Johnson, J. S. *J. Am. Chem. Soc.* **2008**, *130*, 8642−8650. (d) DeAngelis, A.; Taylor, M. T.; Fox, J. M. *J. Am. Chem. Soc.* **2009**, *131*, 1101−1105. (e) Jiang, Z.; Wang, J.; Lu, P.; Wang, Y. *Tetrahedron* **2011**, *67*, 9609−9617. (f) Wu, X.; Li, L.; Zhang, J. *Chem. Commun.* **2011**, *47*, 7824−7826.

(4) For examples of dipolar cycloadditions of oxiranes, see: (a) Bentabed, G.; Derdour, A.; Benhaoua, H. *Synth. Commun.* **2003**, *33*, 1861−1866. (b) Madhushaw, R. J.; Li, C. L.; Su, H. L.; Hu, C. C.; Lush, S. F.; Liu, R. S. *J. Org. Chem.* **2003**, *68*, 1872−1877. (c) Huo, C. D.; Jia, X. D.; Zhang, W.; Yang, L.; Lu, J. M.; Liu, Z. L. *Synlett.* **2004**, 251−254. (d) Hilt, G.; Bolze, P.; Harms, K. *Chem. Eur. J.* **2007**, *13*, 4312−4325. (e) Pan, J.; Zhang, W.; Zhang, J.; Lu, S. *Tetrahedron Lett.* **2007**, *48*, 2781−2785. (f) Chen, Z. L.; Wei, L.; Zhang, J. L. *Org. Lett.* **2011**, *13*, 1170−1173. (g) Hou, X.-L.; Wu, W.-Q.; Ding, C.-H. *Synlett.* **2012**, *23*, 1035−1038. (h) Wang, L.; Li, Z.; Lu, L.; Zhang, W. *Tetrahedron* **2012**, *68*, 1483−1491.

(5) For reviews of the ring opening of oxiranes, see: (a) Parker, R. E.; Isaacs, N. S. *Chem. Rev.* **1959**, *59*, 737−799. (b) Jacobsen, E. N. *Acc. Chem. Res.* **2000**, *33*, 421−431. (c) Vilotijevic, I.; Jamison, T. F. *Angew. Chem., Int. Ed.* **2009**, *48*, 5250−5281.

(6) For some of our recent examples of chemoselective cycloadditions of aryloxiranyldicarboxylate with aldehyde see: (a) Chen, Z. L.; Wei, L.; Zhang, J. L. *Org. Lett.* **2011**, *13*, 1170−1173. (b) Wang, T.; Wang, C.-H.; Zhang, J. *Chem. Commun.* **2011**, *47*, 5578−5580. (c) Chen, Z.; Tian, Z.; Zhang, J.; Ma, J.; Zhang, J. *Chem. Eur. J.* **2012**, *18*, 8591−8595.

(7) For a general review and discussion, see: (a) Kuznetsov, M. L. *Russ. Chem. Rev.* **2006**, *75*, 1045−1073. (b) Ess, D. H.; Houk, K. N. *J. Am. Chem. Soc.* **2008**, *130*, 10187−10198.

(8) (a) Sustmann, R. *Tetrahedron Lett.* **1971**, *12*, 2721−2724. (b) Sustmann, R. *Tetrahedron Lett.* **1971**, *12*, 2717−2720.

(9) For some recent theoretical investigations on regioselective [3 + 2] cycloadditions, see: (a) Li, Z. M.; Wang, Q. R. *Int. J. Quantum Chem.* **2008**, *108*, 1067−1075. (b) Benchouk, W.; Mekelleche, S. M.; Aurell, M. J.; Domingo, L. R. *Tetrahedron* **2009**, *65*, 4644−4651. (c) Cheng, Y.; Wang, B.; Wang, X. R.; Zhang, J. H.; Fang, D. C. *J. Org. Chem.* **2009**, *74*, 2357−2367. (d) Domingo, L. R.; Chamorro, E.; Perez, P. *Eur. J. Org. Chem.* **2009**, 3036−3044. (e) Arróniz, C.; Molina, J.; Abás, S.; Molins, E.; Campanera, J. M.; Luque, F. J.; Escolano, C. *Org. Biomol. Chem.* **2013**, *11*, 1640−1649. (f) Rhyman, L.; Abdallah, H. H.; Jhaumeer-Laulloo, S.; Domingo, L. R.; Joule, J. A.; Ramasami, P. *Tetrahedron* **2011**, *67*, 8383−8391. (g) Bentabed-Ababsa, G.; Hamza-Reguig, S.; Derdour, A.; Domingo, L. R.; Sáez, J. A.; Roisnel, T.; Dorcet, V.; Nassar, E.; Mongin, F. *Org. Biomol. Chem.* **2012**, *10*, 8434−8444.

(10) For several recent examples of mechanistic studies on noble metal catalyzed [3 + 2] cycloaddition, see: (a) Menezes, F. M. C.; Kuznetsov, M. L.; Pombeiro, A. J. L. *Organometallics* **2009**, *28*, 6593−6602. (b) Hou, D.-R.; Kuan, T.-C.; Li, Y.-K.; Lee, R.; Huang, K.-W. *Tetrahedron* **2010**, *66*, 9415−9420. (c) Jiao, L.; Lin, M.; Yu, Z. X. *J. Am. Chem. Soc.* **2011**, *133*, 447−461. (d) García-Fandiño, R.; Gulías, M.; Mascareñas, J. L.; Cárdenas, D. J. *Dalton Trans.* **2012**, *41*, 9468−9481. (e) Liu, T.; Han, L.; Liu, Y.; Zhang, D.; Li, W.-Z. *Comput. Theor. Chem.* **2012**, *992*, 97−102. (f) Liu, Y.; Zhang, D.; Bi, S.; Liu, C. *Org. Biomol. Chem.* **2013**, *11*, 336−343. (g) Rodier, F.; Rajzmann, M.; Parrain, J. L.; Chouraqui, G.; Commeiras, L. *Chem. Eur. J.* **2013**, *19*, 2467−2477.

(11) (a) Domingo, L. R.; Arno, M.; Merino, P.; Tejero, T. *Eur. J. Org. Chem.* **2006**, 3464−3472. (b) Zhang, J. S.; Shen, W.; Li, M. *Eur. J. Org. Chem.* **2007**, 4855−4866. (c) Frank, E.; Mucsi, Z.; Zupko, I.; Rethy, B.; Falkay, G.; Schneider, G.; Wolfling, J. *J. Am. Chem. Soc.* **2009**, *131*, 3894−3904. (d) Zamfir, A.; Schenker, S.; Bauer, W.; Clark, T.; Tsogoeva, S. B. *Eur. J. Org. Chem.* **2011**, 3706−3709. (e) Rhyman, L.; Ramasami, P.; Joule, J. A.; Sáez, J. A.; Domingo, L. R. *RSC Adv.* **2013**, *3*, 447−457. (f) Śnieżek, M.; Stecko, S.; Panfil, I.; Furman, B.; Urbańczyk-Lipkowska, Z.; Chmielewski, M. *Tetrahedron: Asymmetry* **2013**, *24*, 89−103.

(12) (a) Bentabed-Ababsa, G.; Derdour, A.; Roisnel, T.; Saez, J. A.; Perez, P.; Chamorro, E.; Domingo, L. R.; Mongin, F. *J. Org. Chem.* **2009**, *74*, 2120−2133. (b) Lan, Y.; Houk, K. N. *J. Am. Chem. Soc.* **2010**, *132*, 17921−17927.

(13) Novikov, R. A.; Balakirev, D. O.; Timofeev, V. P.; Tomilov, Y. V. *Organometallics* **2012**, *31*, 8627−8638.

(14) (a) Shi, F. Q.; Li, X.; Xia, Y.; Zhang, L.; Yu, Z. X. *J. Am. Chem. Soc.* **2007**, *129*, 15503−15512. (b) Liang, Y.; Liu, S.; Xia, Y. Z.; Li, Y. H.; Yu, Z. X. *Chem. Eur. J.* **2008**, *14*, 4361−4373.

(15) Frisch, M. J.; Trucks, G. W.; Schlegel, H. B.; Scuseria, G. E.; Robb, M. A.; Cheeseman, J. R.; Scalmani, G.; Barone, V.; Mennucci, B.; Petersson, G. A.; Nakatsuji, H.; Caricato, M.; Li, X.; Hratchian, H. P.; Izmaylov, A. F.; Bloino, J.; Zheng, G.; Sonnenberg, J. L.; Hada, M.; Ehara, M.; Toyota, K.; Fukuda, R.; Hasegawa, J.; Ishida, M.; Nakajima, T.; Honda, Y.; Kitao, O.; Nakai, H.; Vreven, T.; Montgomery, J. A., Jr.; Peralta, J. E.; Ogliaro, F.; Bearpark, M.; Heyd, J. J.; Brothers, E.; Kudin, K. N.; Staroverov, V. N.; Keith, T.; Kobayashi, R.; Normand, J.; Raghavachari, K.; Rendell, A.; Burant, J. C.; Iyengar, S. S.; Tomasi, J.;

Cossi, M.; Rega, N.; Millam, J. M.; Klene, M.; Knox, J. E.; Cross, J. B.; Bakken, V.; Adamo, C.; Jaramillo, J.; Gomperts, R.; Stratmann, R. E.; Yazyev, O.; Austin, A. J.; Cammi, R.; Pomelli, C.; Ochterski, J. W.; Martin, R. L.; Morokuma, K.; Zakrzewski, V. G.; Voth, G. A.; Salvador, P.; Dannenberg, J. J.; Dapprich, S.; Daniels, A. D.; Farkas, O.; Foresman, J. B.; Ortiz, J. V.; Cioslowski, J.; Fox, D. J. *Gaussian 09, Revision B.01*, Gaussian, Inc.: Wallingford, CT, 2010.

(16) (a) Becke, A. D. *J. Chem. Phys.* **1993**, *98*, 5648−5652. (b) Lee, C.; Yang, W.; Parr, R. G. *Phys. Rev. B* **1988**, *37*, 785−789.

(17) (a) Hay, P. J.; Wadt, W. R. *J. Chem. Phys.* **1985**, *82*, 270−283. (b) Wadt, W. R.; Hay, P. J. *J. Chem. Phys.* **1985**, *82*, 284−298. (c) Hay, P. J.; Wadt, W. R. *J. Chem. Phys.* **1985**, *82*, 299−310.

(18) Zhao, Y.; Truhlar, D. G. *Theor. Chem. Acc.* **2008**, *120*, 215−241.

(19) (a) Tamura, H.; Yamazaki, H.; Sato, H.; Sakaki, S. *J. Am. Chem. Soc.* **2003**, *125*, 16114−16126. (b) Sakaki, S.; Takayama, T.; Sumimoto, M.; Sugimoto, M. *J. Am. Chem. Soc.* **2004**, *126*, 3332−3348.

(20) Fuentealba, P.; Preuss, H.; Stoll, H.; Von Szentpály, L. *Chem. Phys. Lett.* **1982**, *89*, 418−422.

(21) Marenich, A. V.; Cramer, C. J.; Truhlar, D. G. *J. Phys. Chem. B* **2009**, *113*, 6378−6396.

(22) (a) Glendening, E. D.; Reed, A. E.; Carpenter, J. E.; Weinhold, F. *NBO Version 3.1*. (b) Reed, A. E.; Curtiss, L. A.; Weinhold, F. *Chem. Rev.* **1988**, *88*, 899−926. (c) Reed, A. E.; Weinstock, R. B.; Weinhold, F. *J. Chem. Phys.* **1985**, *83*, 735−746.

(23) The activation energy barriers are calculated at the B3LYP/6-31+G(d) level. In experiments, the C−C bond can be cleaved thermally; see: (a) Wang, G. W.; Yang, H. T.; Wu, P.; Miao, C. B.; Xu, Y. *J. Org. Chem.* **2006**, *71*, 4346−4348. (b) Bentabed-Ababsa, G.; Derdour, A.; Roisnel, T.; Saez, J. A.; Domingo, L. R.; Mongin, F. *Org. Biomol. Chem.* **2008**, *6*, 3144−3157. The C−O bond cleavages always occur under photochemical conditions.[4e,h] Thus for the isolated oxiranes, the C−C bond is weaker than the C−O bond.

(24) Yamamoto, H. *Lewis Acids in Organic Synthesis*; Wiley: Hoboken, NJ, 2002.

(25) (a) Pearson, R. G. *J. Am. Chem. Soc.* **1963**, *85*, 3533−3543. (b) Woodward, S. *Tetrahedron* **2002**, *58*, 1017−1050. (c) Olah, J.; De Proft, F.; Veszpremi, T.; Geerlings, P. *J. Phys. Chem. A* **2005**, *109*, 1608−1615.

(26) (a) Olah, G. A.; Kobayashi, S.; Tashiro, M. *J. Am. Chem. Soc.* **1972**, *94*, 7448−7461. (b) Luo, Y. R.; Benson, S. W. *Inorg. Chem.* **1991**, *30*, 1676−1677. (c) Kobayashi, S.; Busujima, T.; Nagayama, S. *Chem. Eur. J.* **2000**, *6*, 3491−3494. (d) Kobayashi, S.; Manabe, K. *Acc. Chem. Res.* **2002**, *35*, 209−217.

(27) Yamamoto, Y. *J. Org. Chem.* **2007**, *72*, 7817−7831.

(28) Shannon, R. D. *Acta Crystallogr., Sect. A* **1976**, *32*, 751−767.